SCIENTIFIC REPORTS

OPEN

A space network structure constructed by tetraneedlelike ZnO whiskers supporting boron nitride nanosheets to enhance comprehensive properties of poly(L-lacti acid) scaffolds

Pei Feng[1,2,3,*], Shuping Peng[1,4,*], Ping Wu[5], Chengde Gao[2], Wei Huang[2], Youwen Deng[6] & Cijun Shuai[2]

In this study, the mechanical strength and modulus of poly(L-lacti acid) (PLLA) scaffolds were enhanced with the mechanical properties of boron nitride nanosheets (BNNSs) and tetraneedlelike ZnO whiskers (T-ZnO$_w$). The adhesion and proliferation of cells were improved as well as osteogenic differentiation of stem cells was increased. Their dispersion statues in PLLA matrix were improved through a space network structure constructed by three-dimensional T-ZnO$_w$ supporting two-dimensional BNNSs. The results showed that the compressive strength, modulus and Vickers hardness of the scaffolds with incorporation of 1 wt% BNNSs and 7 wt% T-ZnO$_w$ together were about 96.15%, 32.86% and 357.19% higher than that of the PLLA scaffolds, respectively. This might be due to the effect of the pull out and bridging of BNNSs and T-ZnO$_w$ as well as the crack deflection, facilitating the formation of effective stress transfer between the reinforcement phases and the matrix. Furthermore, incorporation of BNNSs and T-ZnO$_w$ together into PLLA scaffolds was beneficial for attachment and viability of MG-63 cells. More importantly, the scaffolds significantly increased proliferation and promoted osteogenic differentiation of human bone marrow mesenchymal stem cells (hBMSCs). The enhanced mechanical and biological properties provide the potentials of PLLA/BNNSs/T-ZnO$_w$ scaffolds for the application into bone tissue engineering.

Poly(L-lacti acid) (PLLA) is an attractive scaffold material owing to its biocompatibility and processability, and tunable biodegradability[1–3]. It can completely degrade to carbon dioxide and water by hydrolysis. In addition, PLLA has biological interactions with host cells and can support bone regeneration after implantation. However, the poor mechanical properties hamper its application in the repair of load bearing bone defects[4,5]. Introduction of nano second phase such as nanoparticles, nanotubes, nanosheets and whiskers into polymer matrix is a promising approach to overcome the defects[6–10]. While the enhancing efficiency by these nano second phases in polymers is limited owing to agglomeration[11–13]. In very recent years, the hybridization of one-dimensional nanotubes and two-dimensional nanosheets (or nanoplatelets) has been proposed to promote the dispersion[14–18]. While

[1]Hunan Provincial Tumor Hospital and the Affiliated Tumor Hospital of Xiangya School of Medicine, School of Basic Medical Science, Central South University, Changsha 410013, China. [2]State Key Laboratory of High Performance Complex Manufacturing, the State Key Laboratory for Powder Metallurgy, Central South University, Changsha 410083, China. [3]State Key Laboratory of Solidification Processing, Northwestern Polytechnical University, Xi'an 710072, China. [4]School of Basic Medical Science, Central South University, Changsha 410078, China. [5]College of Chemistry, Xiangtan University, Xiangtan 411105, China. [6]Department of Orthopedics, The Second Xiangya Hospital, Central South University, Changsha 410011, China. *These authors contributed equally to this work. Correspondence and requests for materials should be addressed to C.S. (email: shuai@csu.edu.cn)

carbon nanotubes are easily attached in the direction paralleling to graphene surface because of the strong π-π stacking interaction between the two materials.

Herein, a space network structure is constructed by three-dimensional tetraneedlelike ZnO whiskers (T-ZnO$_w$) in cooperation with boron nitride nanosheets (BNNSs). In this space network structure, T-ZnO$_w$ can support BNNSs in the direction perpendicular to the surface, which is beneficial to the dispersion of each other more effectively. Boron nitride (BN), so-called "white graphite", is a two-dimensional layered material that exhibits a hexagonal crystal structure. BNNSs possess elastic modulus (505–1031 GPa) and tensile strength (>150 GPa), which provides them potential reinforcement for strengthening of polymer scaffold[19,20]. Another important consideration for using BNNSs in bone tissue engineering is their good biocompatibility. Previous studies have shown that BN exhibited non-cytotoxic and good cytocompatibility to osteoblasts, macrophages, human embryonic kidney cells and neuroblastoma cells[21–24]. In addition, it could promote the differentiation of mesenchymal stem cells (MSCs) into osteoblasts[25].

T-ZnO$_w$, a new kind of whiskers with a single crystal, have been used as an ideal reinforcement to improve the mechanical properties of polymer because of the super high strength and modulus[26,27]. They exhibit needle-like tetrapod shapes with four needle-like arms extending from the same center in four directions in three-dimensional space, which leads to a homogeneous stress distribution in the polymer matrix[28]. Niu *et al.* added T-ZnO$_w$ to resin composite and found that the addition of T-ZnO$_w$ could improve the flexural, compressive and tensile strength of resin composite[29]. Apart from this, ZnO was biocompatible and could promote cell adhesion and growth[30,31]. Additionally, some studies reported that ZnO had bioactive and could facilitate apatite formation after soaking in simulated body fluid (SBF)[32,33].

Therefore, besides the constructing of the space network structure to promote dispersion in PLLA matrix, there are another two aims for using of BNNSs and T-ZnO$_w$ together, namely: (i) to enhance the compressive strength, modulus and Vickers hardness of PLLA scaffold with the advantage of their mechanical properties, and (ii) to improve the cell attachment, proliferation and differentiation abilities with the advantage of their biological properties.

Results

The images for the original powder, PLLA scaffold and PLLA/BN/ZnO scaffold are shown in Fig. 1. PLLA powder have irregular shape with the particle size from 0.2 to 5 μm (Fig. 1a). BNNSs powder has platelet form and the morphology is uniform (Fig. 1c). T-ZnO$_w$ powder has tetraneedlelike nanostructure, and the four needlelike arms extend from the same center in four directions (Fig. 1d). The BNNSs and T-ZnO$_w$ powder were randomly dispersed with PLLA powder, and individual T-ZnO$_w$ was clearly seen and maintained its original morphology in composite powder after mixing (Fig. 1e). The composite powder was sintered on a SLS system for fabricating porous scaffolds, and the sintering process was described in our previous study[34]. All the scaffolds had uniform macropores with interconnected pore channels and the pore size was around 800 μm (Fig. 1b,f). The size of scaffolds was about 13.5 mm × 13.5 mm × 7 mm and there was no significant difference between the PLLA scaffold and the PLLA/BN/ZnO scaffold.

Mechanical properties (compressive strength, modulus and Vickers hardness) of the scaffolds with BNNSs or T-ZnO$_w$ at different content were measured (Fig. 2). The compressive strength, modulus and Vickers hardness first increased with BNNSs content increasing from 0 to 0.75 wt% and then decreased with BNNSs content further increasing to 1.25 wt% (Fig. 2a,b). The highest compressive strength, modulus and Vickers hardness were 28.17 MPa, 2.85 GPa and 164.76 MPa, respectively. The compressive strength, modulus and Vickers hardness of the PLLA/ZnO scaffolds increased from 17.41 MPa, 2.13 GPa and 53.19 MPa to 25.72 MPa, 2.64 GPa and 127.71 MPa with T-ZnO$_w$ content increasing from 0 to 5 wt%, respectively (Fig. 2c,d). And then decreased to 24.16 MPa, 2.43 GPa and 112.75 MPa with T-ZnO$_w$ content further increasing to 9 wt%.

The mechanical properties of the PLLA, PLLA/BN-0.75, PLLA/ZnO-5, PLLA/BN/ZnO-0.75-5 and PLLA/BN/ZnO-1-7 scaffolds are shown in Fig. 3. The PLLA/BN/ZnO-0.75-5 scaffolds had higher compressive strength, modulus and Vickers hardness than the PLLA, PLLA/BN-0.75 and PLLA/ZnO-5 scaffolds, which indicated that the addition of BNNSs and T-ZnO$_w$ together in the PLLA matrix resulted in the higher mechanical properties than that of addition of BNNSs or T-ZnO$_w$ individually ($p < 0.01$). The compressive strength, modulus and Vickers hardness of the PLLA/BN/ZnO-1-7 scaffolds were higher than that of the PLLA/BN/ZnO-0.75-5 scaffolds and about 96.15%, 32.86% and 357.19% higher than that of the PLLA scaffolds, respectively.

The surface morphologies and the corresponding schematic of BNNSs and T-ZnO$_w$ dispersion in the PLLA matrix are shown in Fig. 4. A homogeneous dispersion of BNNSs throughout the PLLA matrix was achieved at lower BNNSs content, such as 0.75 wt% (Fig. 4a1,b1). While part of the BNNSs aggregated at higher content (1 wt%) because of the great specific surface area (Fig. 4a2,b2). For the PLLA/ZnO scaffolds, T-ZnO$_w$ were well dispersed in the matrix when the content was 5 wt% (Fig. 4a3,b3), while further increased the content led to the poor dispersion due to the strong van der Waals interactions (Fig. 4a4,b4). The poor dispersion of BNNSs and T-ZnO$_w$ in PLLA matrix would result in some defects on the scaffolds surface, which decreased the overall mechanical properties[35–37]. However, the dispersion state of BNNSs and T-ZnO$_w$ in the matrix was improved by incorporation of BNNSs and T-ZnO$_w$ together into PLLA matrix (Fig. 4a5,b5). The reason was that two-dimensional BNNSs and three-dimensional T-ZnO$_w$ could construct a space network structure which exhibited a synergetic enhancing effect on the mechanical properties of scaffolds. In the structure, T-ZnO$_w$ could support the BNNSs in the direction perpendicular to the surface, which might be beneficial to the dispersion of each other more effectively. This structure could be further observed from the fracture images of the scaffolds.

The XRD spectra of the PLLA, PLLA/BN, PLLA/ZnO and PLLA/BN/ZnO scaffolds are shown in Fig. 5. The results of the original PLLA, BNNSs and T-ZnO$_w$ powder were also provided for comparison. It could be seen that PLLA powder had two diffraction peaks at 2θ = 16.3° and 18.6°, while the diffraction peaks of BNNSs and T-ZnO$_w$ were 26.8°, 41.8°, and 31.8°, 34.4°, 36.3°, 47.5°, respectively. The peaks of other impurity phases were not
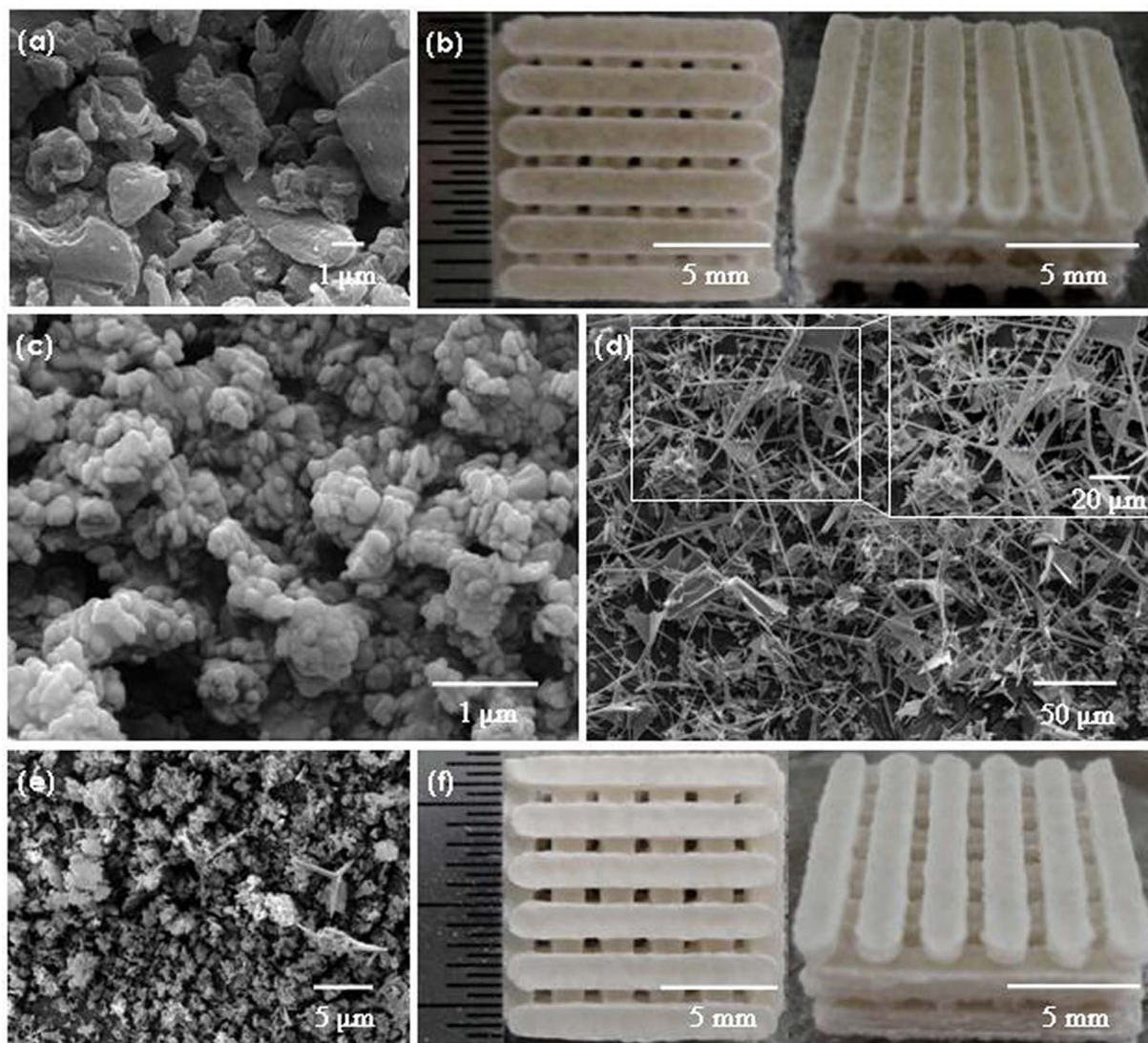
Figure 1. SEM and Optical images. SEM images for (**a**) PLLA powder, (**c**) BNNSs powder, (**d**) T-ZnO_w powder, (**e**) Composite powder, and Optical images for the (**b**) PLLA scaffold and (**f**) PLLA/BN/ZnO scaffold.

found. In addition to the stacked peaks of PLLA and BNNSs, no other peaks were observed in the PLLA/BN-0.75 scaffolds. Similarly, no new peak was found in the PLLA/ZnO-5 scaffolds either. The pattern of PLLA/BN/ZnO-0.75-5 and PLLA/BN/ZnO-1-7 scaffolds still retained the same profile as observed in the PLLA scaffolds, and the additional diffraction peaks at 26.8°, 41.8°, and 31.8°, 34.4°, 36.3°, 47.5° corresponded to BNNSs and T-ZnO$_w$, respectively. These results indicated that BNNSs and T-ZnO$_w$ still existed and there was no new phase formed in the PLLA/BN, PLLA/ZnO and PLLA/BN/ZnO scaffolds after laser sintering.

To evaluate the response of cells to the scaffolds, MG-63 cells were seeded and cultured onto the PLLA, PLLA/BN-0.75, PLLA/ZnO-5, PLLA/BN/ZnO-0.75-5 and PLLA/BN/ZnO-1-7 scaffolds for 7 days, and their adhesion, viability and proliferation were studied (Fig. 6). MG-63 cells could adhere to all types of scaffolds, indicating the good cytocompatibility. More cells attached on the PLLA/BN and PLLA/ZnO scaffolds than on the PLLA scaffolds (Fig. 6a1), and some cells started to spread out with cytoplasmic bridges between them (Fig. 6b1,c1). The cells were spreading well and almost completely covered the PLLA/BN/ZnO scaffolds surface, especially the PLLA/BN/ZnO-1-7 scaffolds (Fig. 6d1,e1). In the fluorescence images, live cells were stained green, while dead cells were stained red, respectively. The cells were uniformly distributed on all the scaffolds, indicating the scaffold materials were homogenous. They grew well on the PLLA/BN/ZnO scaffolds and spread to the whole areas of the scaffold surface, while the PLLA scaffolds had the lowest number of live cells. The increased cell attachment and viability of the PLLA/BN/ZnO scaffolds suggested that the addition of BNNSs and T-ZnO$_w$ had positive effect on cell response.

An ideal scaffold should not only have appropriate mechanical properties and cytocompatibility, but also be able to degrade at appropriate rate. Thus, the degradation behavior of the PLLA and PLLA/BN/ZnO-1-7 scaffolds was investigated in PBS solution, as shown in Fig. 7. The scaffolds before soaking in PBS had a flat, smooth and
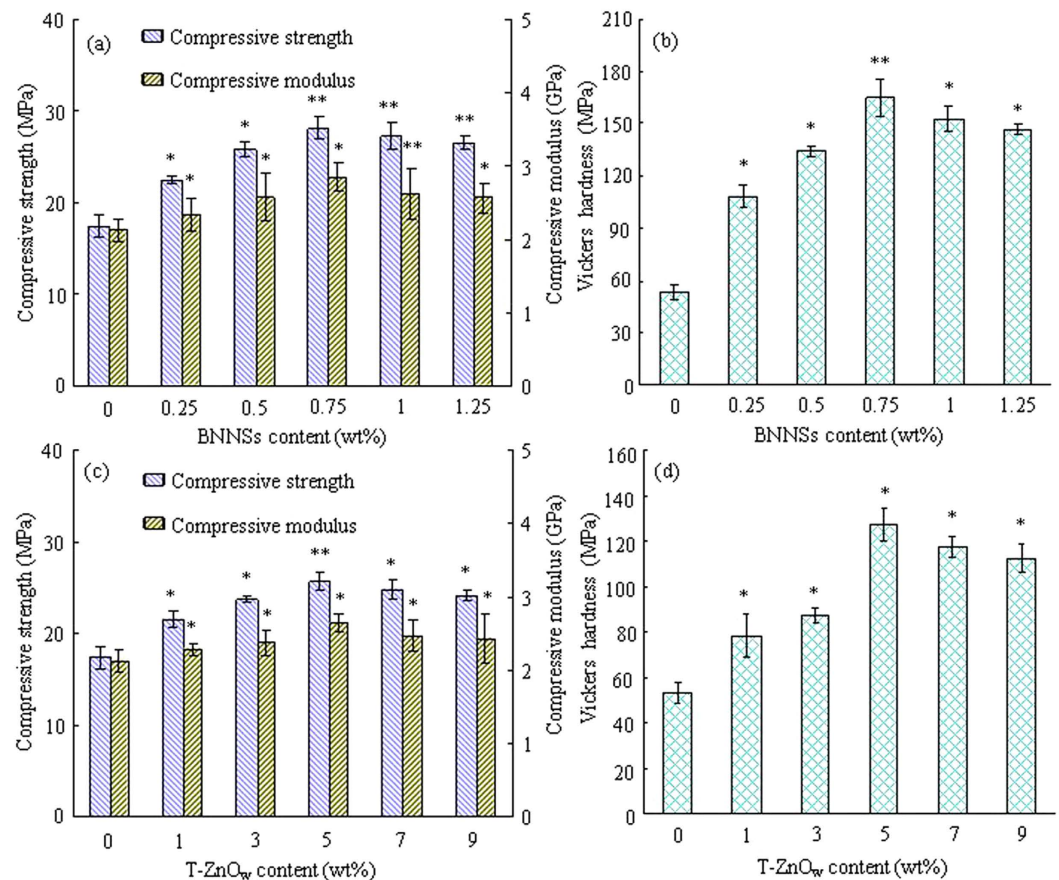
Figure 2. The analysis of compressive strength, modulus and Vickers hardness of scaffolds. (a,b) PLLA/
BN scaffolds; (**c,d**) PLLA/ZnO scaffolds. *Represents significant difference (*p < 0.05*) and **represents very
significant difference (*p < 0.01*) when the PLLA/BN or PLLA/ZnO scaffolds, as compared to the PLLA scaffolds.

dense surface (Fig. 7a). The PLLA and PLLA/BN/ZnO-1-7 scaffolds could degrade in PBS and the degradation
degree increased with the soaking time (Fig. 7b1–b4,c1–c4). The PLLA scaffolds degraded faster than the PLLA/
BN/ZnO-1-7 scaffolds and a large area of degradation was observed after 14 days of soaking or more time. It had
8.51% weight loss after 28 days of immersion, while the PLLA/BN/ZnO-1-7 scaffolds displayed a slower degrada-
tion rate with 7.17% weight loss during the same immersion time (Fig. 7d), which indicated that the addition of
BNNSs and T-ZnO$_w$ contributed a higher resistance to degradability of PLLA scaffolds. The result was in agree-
ment with report by Şen *et al.*[38], who found that the biodegradation of the gelatin-glucose scaffolds including BN
was slower than the gelatin-glucose scaffolds without BN. Previous studies also showed that ZnO did not degrade
in biological environment[39], and could slow down the degradation rate[40].

The attachment and proliferation of hBMSCs cultured on the PLLA and PLLA/BN/ZnO-1-7 scaffolds were
determined by SEM analysis and MTT assay, respectively, as shown in Fig. 8. HBMSCs adhered on PLLA/BN/
ZnO-1-7 scaffolds as well as the PLLA scaffolds and began to spread after 3 days of incubation. The cells on the
two scaffolds proliferated over the culture time. The PLLA/BN/ZnO-1-7 scaffolds had a faster cell proliferation
rate than the PLLA scaffolds, which indicated that the incorporation of BNNSs and T-ZnO$_w$ into PLLA greatly
facilitated hBMSCs proliferation. The differentiation of hBMSCs cultured on the PLLA and PLLA/BN/ZnO-1-7
scaffolds for 1, 3, 5 and 7 days was assessed in terms of ALP activity, as shown in Fig. 9. The ALP activity was
increased in both PLLA and PLLA/BN/ZnO-1-7 scaffolds with increased incubation time. Similar to the cell
proliferation results, the ALP activity of mesenchymal stem cells on the PLLA/BN/ZnO-1-7 scaffolds was higher
than that on the PLLA scaffolds, indicating the significant up-regulated osteogenic differentiation of the cells.

Discussion
Mechanical properties of scaffold are important factors in bone tissue engineering application because scaffold
should withstand stress during culturing and implanting[41]. The mechanical properties of the PLLA/BN and
PLLA/ZnO scaffolds were significant higher than that of the PLLA scaffolds (*p < 0.05*). The results showed that
the addition of BNNSs or T-ZnO$_w$ enhanced the mechanical properties of PLLA scaffolds, while the enhancement
efficiency was highly depended on the fillers content (Fig. 2). For example, the compressive strength, modulus
and Vickers hardness of the PLLA/BN scaffolds increased with BNNSs content increasing from 0 to 0.75 wt% and
then decreased with BNNSs content further increasing to 1.25 wt% (Fig. 2a,b). While the mechanical properties
of the PLLA/ZnO scaffolds increased with T-ZnO$_w$ content increasing from 0 to 5 wt% and then decreased with
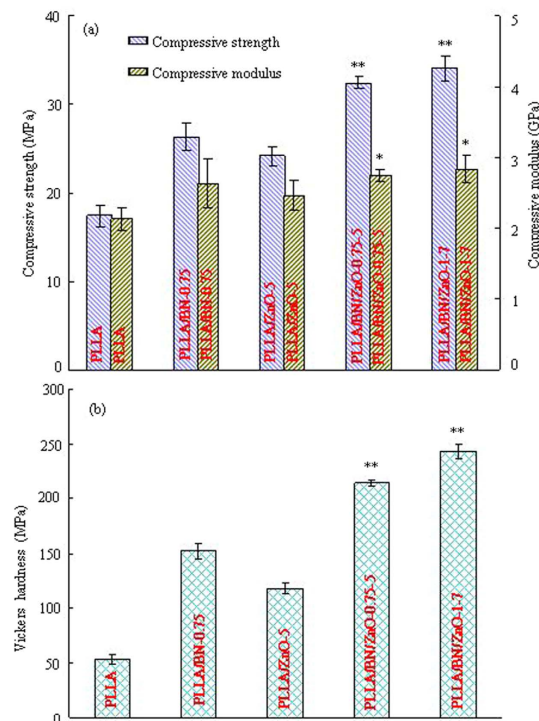
Figure 3. The compressive strength and modulus, and Vickers hardness of the scaffolds. (a) Compressive strength and modulus; **(b)** Vickers hardness. *Represents significant difference ($p < 0.05$) and **represents very significant difference ($p < 0.01$) when the PLLA/BN/ZnO scaffolds, as compared to the PLLA, PLLA/BN-0.75 and PLLA/ZnO-5 scaffolds.

T-ZnO$_w$ content further increasing to 9 wt% (Fig. 2c,d). The mechanical properties decreased due to the agglomeration of fillers. Previous studies demonstrated that the agglomeration of BNNSs or T-ZnO$_w$ in polymer matrix decreased the mechanical properties[42,43]. The compressive strength, modulus and Vickers hardness of the PLLA/BN/ZnO-1-7 scaffolds were higher than that of the PLLA/BN/ZnO-0.75-5 scaffolds and about 96.15%, 32.86% and 357.19% higher than that of the PLLA scaffolds, respectively. A comparison of the increase in the strength, modulus and hardness of PLLA/BN/ZnO-1-7 scaffolds with PLLA composite with different reinforcement phase reported in the literatures[44–53] are shown in Table 1. Although the scaffolds fabricated by SLS were porous structure, the mechanical properties laid in the same range as that of the composite fabricated by different method with different fillers. As we know, the mechanical properties decreased with the increase of porosity for porous materials[54,55].

To investigate the reasons behind the mechanical properties enhancements, further studies were conducted to study the fracture images of PLLA/BN/ZnO scaffolds, as shown in Fig. 10. The fracture images revealed that the surface was quite smooth, which was the typical characteristic of brittle fracture behavior of PLLA[56]. T-ZnO$_w$ with one needle pinning into the matrix and the other three needles pulled out from the matrix was observed (Fig. 10a). They were embedded in the PLLA matrix and only some of the needles could be observed (Fig. 10b). If one needle of the T-ZnO$_w$ was pulled out from the matrix, the other three needles that embedded into the matrix had a role of anchor. Hole was observed because of the pullout of T-ZnO$_w$ from PLLA matrix, indicating the strong interfacial interaction between T-ZnO$_w$ and matrix (Fig. 10c)[57,58]. BNNSs pull out were visible, and some T-ZnO$_w$ attached to BNNSs surface (Fig. 10d), which was an evidence for synergetic effect between BNNSs and T-ZnO$_w$. BNNSs and T-ZnO$_w$ could act as bridges and restrict the widening of crack (Fig. 10e), which increased the energy required to open the crack[59–61]. The propagation direction of the crack was altered and the crack deflection occurred when crack propagation encountered the T-ZnO$_w$ (Fig. 10f). EDS analysis confirmed that the phase at point A and B were BN and ZnO, respectively.

It is known to us that cell behavior on the scaffold is influenced primarily by the chemical composition. Previous studies have already showed that PLLA could support osteoblast adhesion, spreading and growth[62,63]. In this study, the PLLA scaffolds could support MG-63 cell adhesion as well as migration, which suggested the good cytocompatibility of the material for bone scaffolds. Incorporation of BNNSs and T-ZnO$_w$ into PLLA did not alter the major chemical composition. While introduction of Zn element into scaffolds is conducive to the improvement of osteoblast activity and bone formation[64,65]. In addition, it has been confirmed that BN possesses good cytocompatibility to human neuroblastoma cell, osteoblasts, macrophages, and so on[66–68]. For example, Lahiri et al.[67] added boron nitride nanotubes (BNNTs) to biodegradable polylactide polycaprolactone (PLC) copolymer and found that PLC-BNNT composites exhibited increased osteoblast viability than that of PLC.

The attachment and proliferation of hBMSCs on the scaffolds of PLLA and PLLA/BN/ZnO-1-7 increased with culture time, indicating good cytocompatibility. Moreover, the proliferation of hBMSCs on the PLLA/BN/
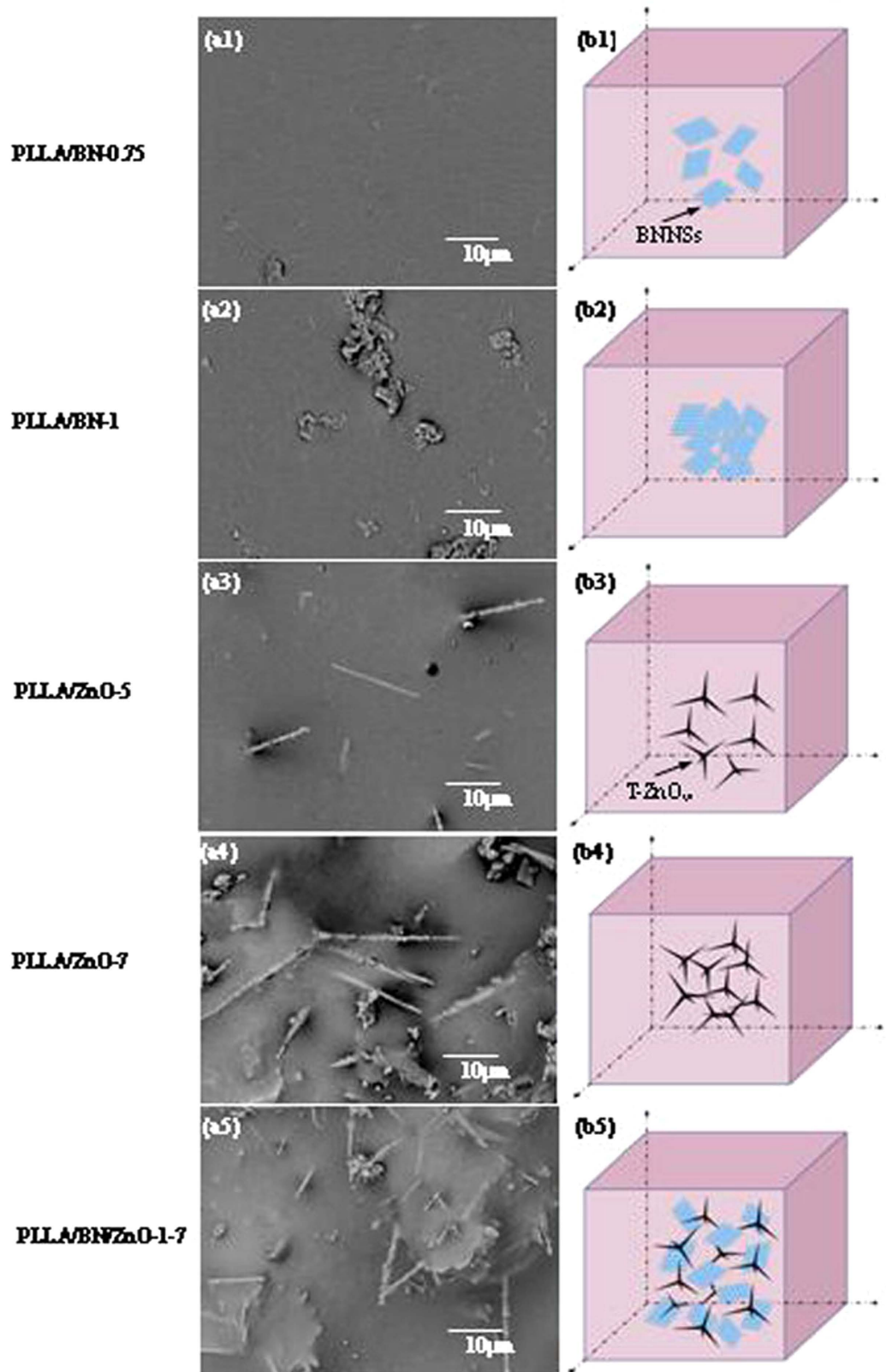
Figure 4. The morphologies and corresponding schematic. The morphologies (**a1–a5**) of the scaffolds under SEM and the corresponding schematic (**b1–b5**) of BNNSs and T-ZnO$_w$ dispersion in the PLLA matrix.

ZnO-1-7 scaffolds was significantly higher than PLLA scaffolds, indicating that the PLLA/BN/ZnO-1-7 scaffolds significantly promoted the cell proliferation. The ALP activity of hBMSCs cultured on the scaffolds increased with
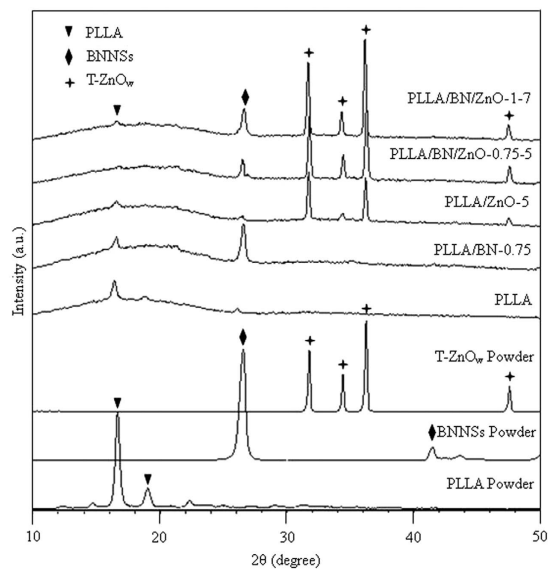
Figure 5. XRD spectra of PLLA, BNNSs and T-ZnO$_w$ powder, and the PLLA, PLLA/BN-0.75, PLLA/ZnO-5, PLLA/BN/ZnO-0.75-5 and PLLA/BN/ZnO-1-7 scaffolds.

culture time, and the ALP activity of the cells on PLLA/BN/ZnO-1-7 scaffolds was significantly higher than PLLA scaffolds. The results revealed that the PLLA/BN/ZnO-1-7 scaffolds could promote cell osteogenic differentiation. It indicated that the addition of BNNSs and T-ZnO$_w$ into PLLA scaffolds was beneficial to hBMSCs proliferation and differentiation, which played a critical role in new bone formation and growth. One possible reason for the improved cell proliferation and differentiation was that the addition of BNNSs into scaffold was beneficial for the expression of several essential cell adhesion proteins (such as fibronectin or vitronectin) during cell culture, which promoted cell adhesion and further increased cell proliferation and differentiation[69,70]. A recent study had shown that BN could result in an increase in the Runx2 gene expression level, indicating the increased osteogenic differentiation[67]. In addition, Zn ion could release from scaffold degradation and stimulate mesenchymal stem cells proliferation and differentiation into osteoblast[71,72].

Conclusions

In the presented work, two-dimensional BNNSs and three-dimensional T-ZnO$_w$ were incorporated into PLLA matrix together to improve the comprehensive properties of scaffold fabricated by SLS. T-ZnO$_w$ supported the interlayers of boron nitride in the direction perpendicular to BNNSs surface during the mixing process, helping their homogenous dispersion within the PLLA matrix. The optimal compressive strength, modulus and Vickers hardness of the scaffolds were obtained at a hybrid addition of 1 wt% BNNSs and 7 wt% T-ZnO$_w$. Strengthening mechanisms were attributed to the formation of effective stress transfer between BNNSs, T-ZnO$_w$ and the matrix due to BNNSs and T-ZnO$_w$ pull out and bridging as well as the crack deflection. In addition, *in vitro* cell culture assays demonstrated that MG-63 cell and hBMSCs could attach, grow and spread on the scaffolds, and incorporation of BNNSs and T-ZnO$_w$ together into PLLA scaffolds could promote MG-63 cell attachment and viability and enhance hBMSCs proliferation and differentiation. Overall, all these results indicated that the fabricated PLLA/BNNSs/T-ZnO$_w$ scaffolds were promising candidates for bone tissue engineering.

Materials and Methods

Materials and reagents. PLLA was supplied by Jinan Daigang Biomaterial Co., Ltd. (Jinan, China) in powder form ($M_w \sim 10$ kDa, $T_g = 60$–$65\,°C$, $T_m = 175$–$185\,°C$). BNNSs were provided by Nanjing XFNANO Materials Tech Co., Ltd. (Nanjing, China) (diameter: 0.5–5 μm, thickness: <50 nm, and purity: >99.5%). T-ZnO$_w$ was obtained from Hefei Yijia New Materials Technology Co., Ltd. (Hefei, China) (needles length: 5–10 μm, needles diameter: 0.5 μm, and purity: >99%). MG-63 cells and hBMSCs were bought from the American Type Culture Collection (Rockville, MD). Dulbecco's modified eagle's medium (DMEM) and fetal bovine serum (FBS) were obtained from Gibco (CA, USA). 3-(4,5-dimethylthiazol-2-yl)-2,5-diphenyltetrazolium bromide (MTT) and dimethyl sulfoxide (DMSO) were purchased from Grand Island Biological Co. (Qingdao, China). All other chemicals and reagents were obtained from Sigma Aldrich (Beijing, China) and used as received.

Preparation of the porous scaffolds. PLLA/BNNSs and PLLA/T-ZnO$_w$ composite powder were prepared by ultrasonic dispersion followed by magnetic filtration, which involves (a) dispersing of PLLA/ethyl alcohol for 30 min with a SK3300H ultrasonic cleaning device (Shanghai Kudos Ultrasonic Instrument Co., Ltd., China), (b) adding appropriate amount of BNNSs and T-ZnO$_w$ to the PLLA solution and continuing dispersing for another 30 min, respectively, (c) stirring the solution with a JB-5 magnetic stirrer (Jintan Ronghua Instrument Manufacture Co., Ltd., China), (d) filtering the solution and then drying overnight in 101-00S electrothermal
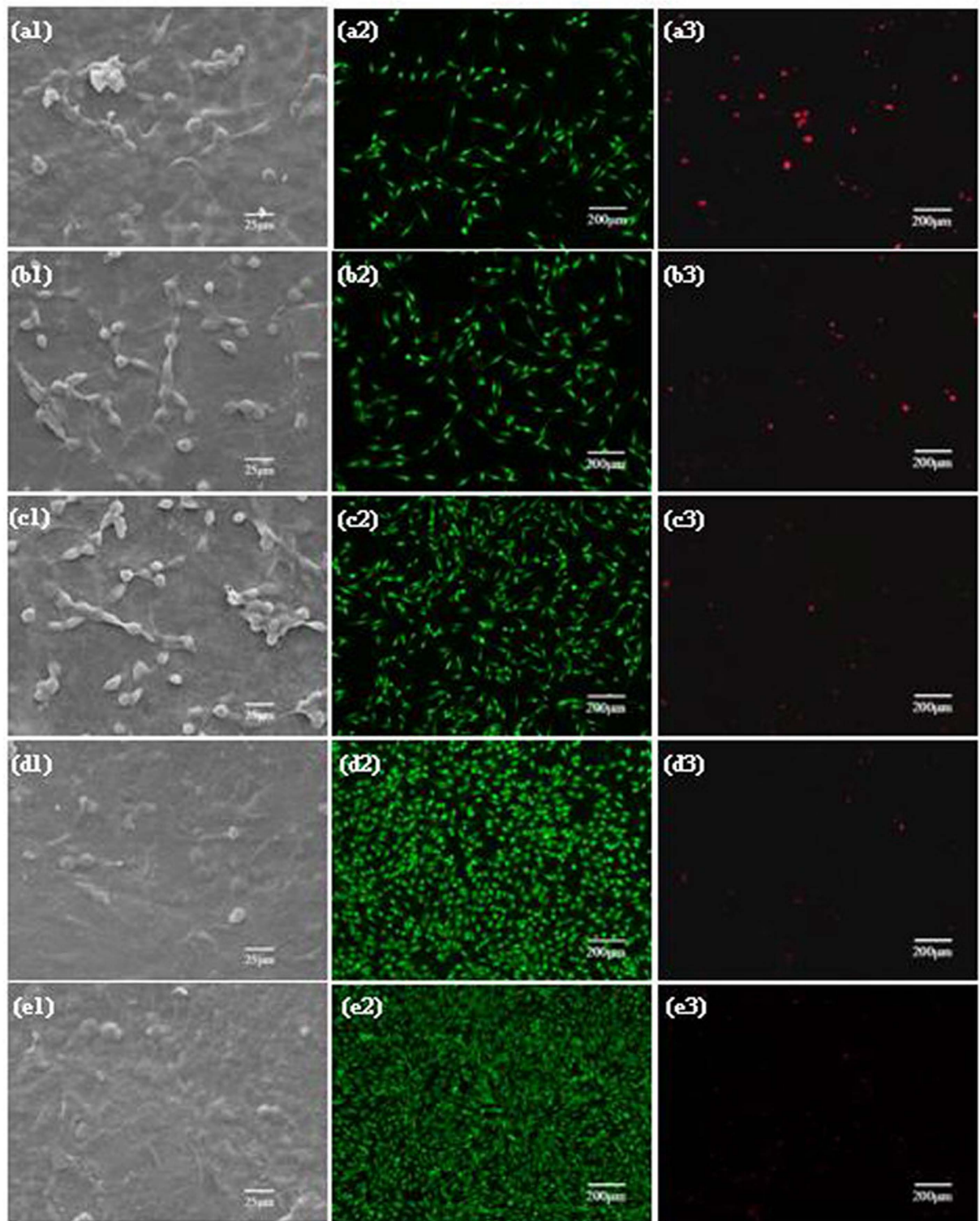
Figure 6. The viability of MG-63 cells on the scaffolds after 7 days of culture. (**a1–a3**) PLLA scaffolds; (**b1–b3**) PLLA/BN-0.75 scaffolds; (**c1–c3**) PLLA/ZnO-5 scaffolds; (**d1–d3**) PLLA/BN/ZnO-0.75-5 scaffolds; (**e1–e3**) PLLA/BN/ZnO-1-7 scaffolds; (**a1,b1,c1,d1,e1**) the SEM images; (**a2,b2,c2,d2,e2**) live cells were stained green; (**a3,b3,c3,d3,e3**) dead cells were stained read. The fluorescence images were acquired using the same camera at the same level of excitation light.

blowing dry box (Guangzhou Dayang Electronic Machinery Equipment Co., Ltd., China). Similarly, PLLA/BNNSs/T-ZnO$_w$ composite powder was also prepared using the same method.
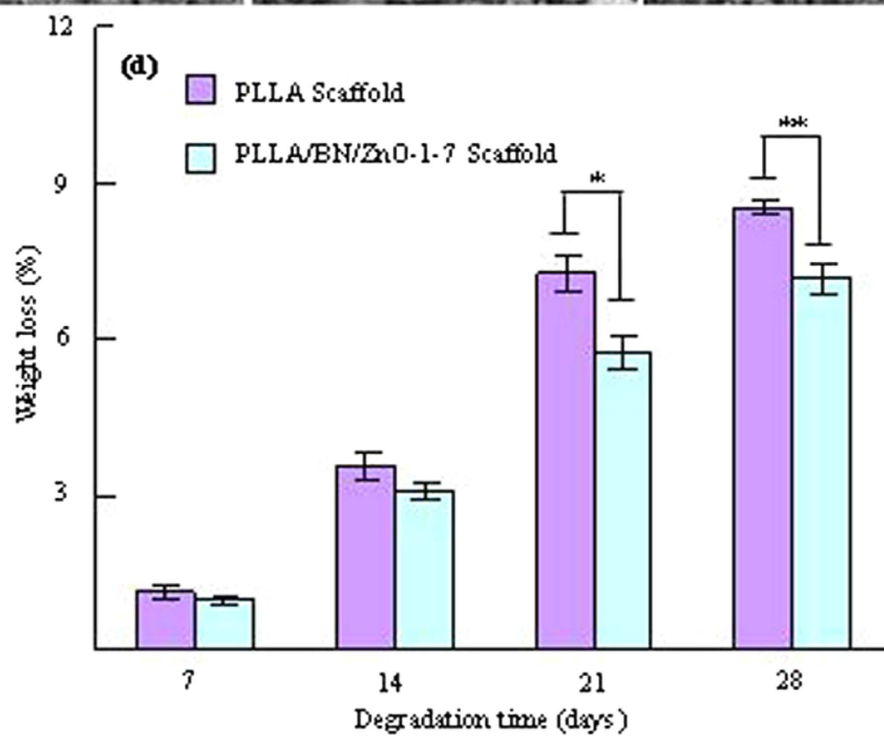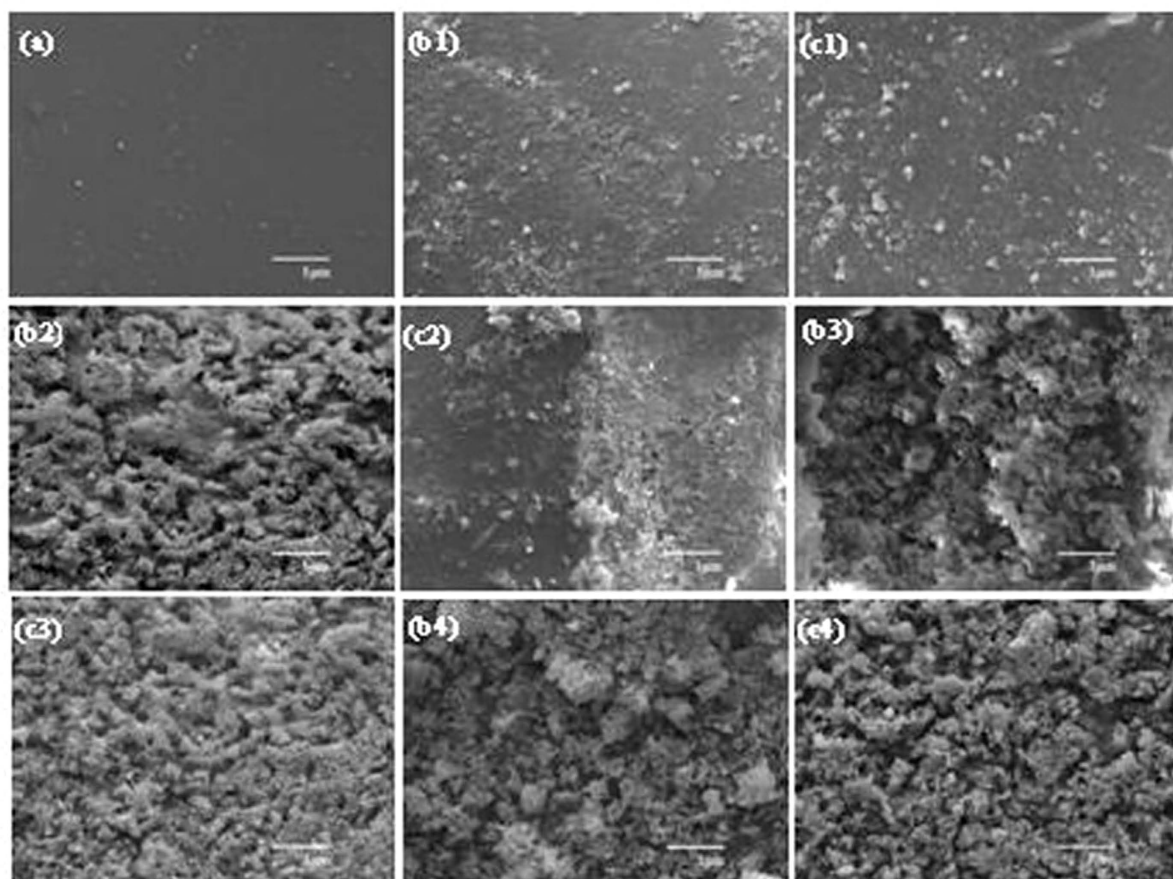
Figure 7. The morphologies of the scaffolds before and after soaked in PBS and weight loss. SEM images (**a,b1,c1, b2,c2,b3,c3,b4,c4**) and weight loss (**d**) of the PLLA (**a,b1,b2,b3,b4**) and PLLA/BN/ZnO-1-7 (**a,c1,c2,c3,c4**) scaffolds before (**a**) and after soaking in PBS for 7 (**b1,c1**), 14 (**b2,c2**), 21 (**b3,c3**) and 28 (**b4,c4**) days (*p < 0.05, **p < 0.01).
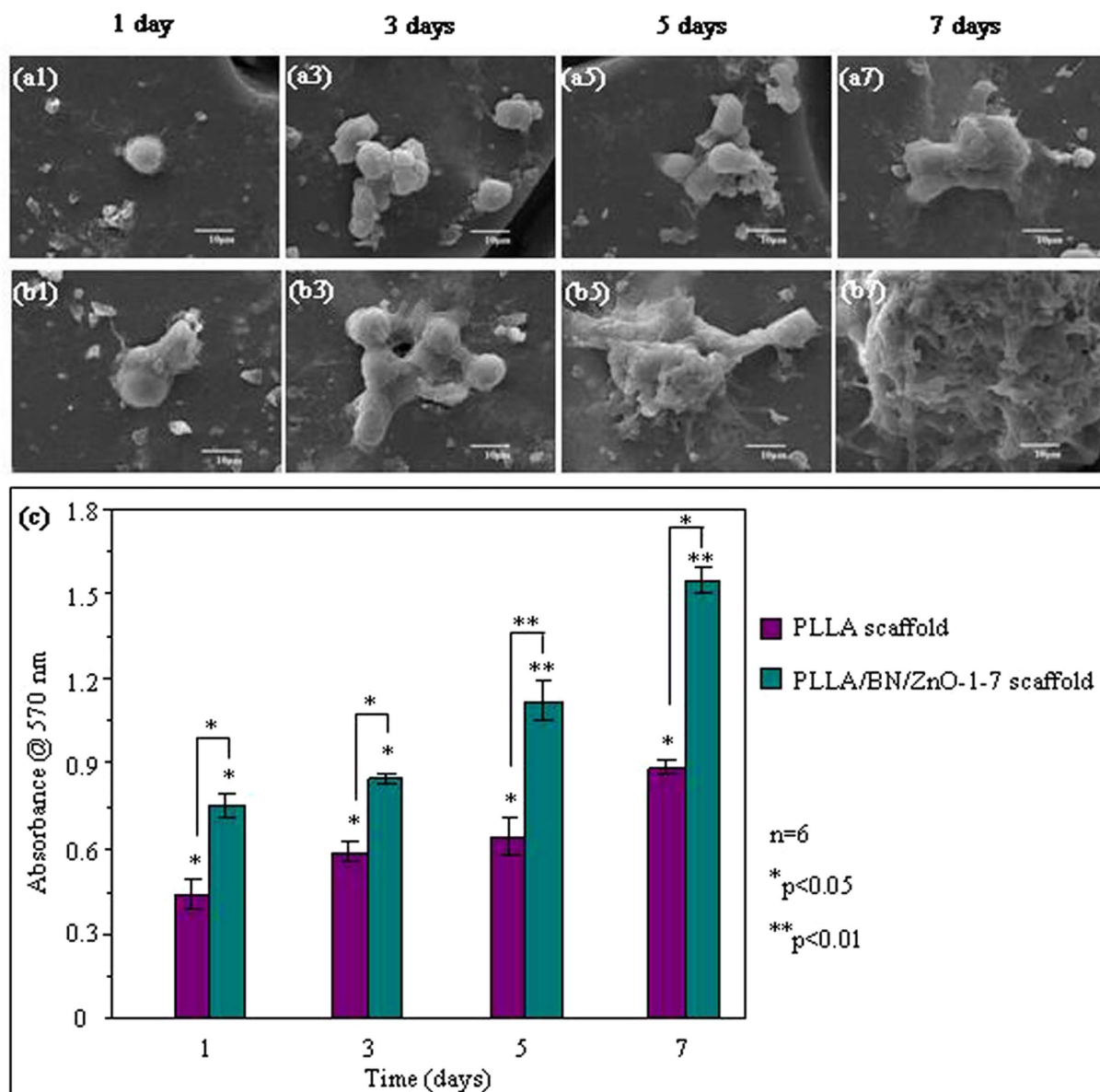
Figure 8. Attachment and proliferation of the hBMSCs cultured on the scaffolds for different periods. SEM images (**a1,a3,a5,a7,b1,b3,b5,b7**) and MTT assay (**c**) of the hBMSCs cultured on the PLLA (**a1,a3,a5,a7**) and PLLA/BN/ZnO-1-7 (**b1,b3,b5,b7**) scaffolds.

Porous scaffolds were fabricated by selective laser sintering (SLS) using a 100 W CO_2 laser ($\lambda = 10.6\,\mu m$). The composite powder was sintered at the following optimized parameters: laser power of 3 W, scanning speed of 400 mm/min, spot diameter of 1 mm and bed temperature of 50 °C. The PLLA/BNNSs and PLLA/T-ZnO_w scaffolds were designated as PLLA/BN-x and PLLA/ZnO-y, respectively, and the PLLA/BNNSs/T-ZnO_w scaffolds were designated as PLLA/BN/ZnO-x-y, in which x and y were the weight percentage of BNNSs and T-ZnO_w content, respectively. For example, PLLA/BN/ZnO-1-7 means that the BNNSs and T-ZnO_w content in the scaffolds was 1 wt% and 7 wt%, respectively.

Characterization of the scaffolds. The morphologies of the powder and scaffolds were observed using a FEI Quanta-200 scanning electron microscopy (SEM, FEI Co., USA). To observe the internal structures of scaffolds, the samples were frozen in liquid nitrogen for 8 min and then broken open using forceps. All specimens were sputter-coated with gold-palladium using a JFC-1600 auto fine coater (JEOL Ltd., Japan). The phase composition was determined by D8 Advance X-ray diffraction (XRD, German Bruker Co., German). The Cu-Kα nickel filtered radiation was detected at a 2θ angle range of 10–50 degrees. The compressive properties of scaffolds were measured using WD-D1 universal testing machine (Shanghai Zhuoji Instruments Co. Ltd., China) at a crosshead displacement speed of 0.5 mm/min. Six specimens (10 mm × 10 mm × 5 mm) were tested against each set. Vickers indentation tests were performed on the specimen (1 mm × 1 mm × 1 mm) surface to evaluate the
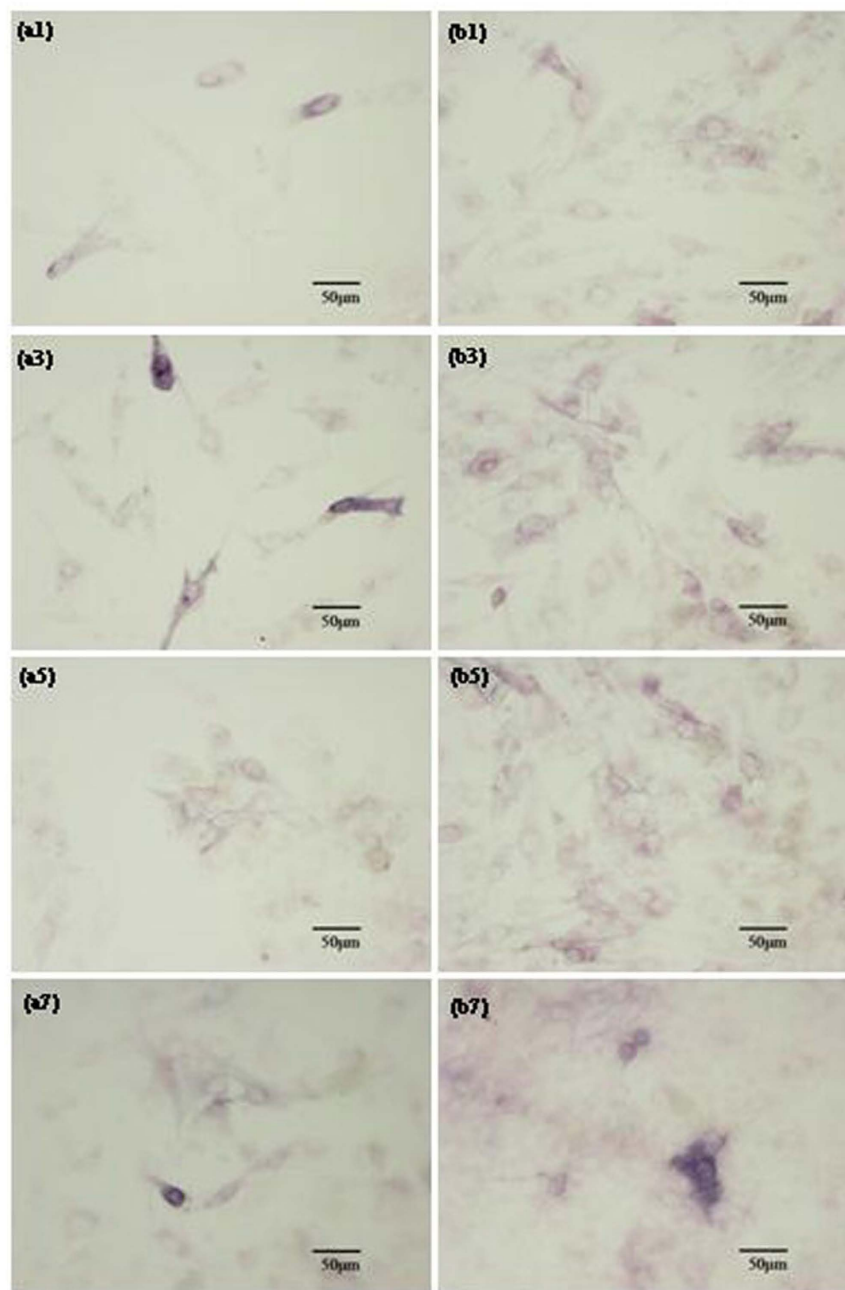
Figure 9. Osteoblastic differentiation of hBMSCs cultured on the scaffolds. ALP activities of hBMSCs cultured on the PLLA (**a1,a3,a5,a7**) and PLLA/BN/ZnO-1-7 (**b1,b3,b5,b7**) scaffolds for 1 (**a1,b1**), 3 (**a3,b3**), 5 (**a5,b5**) and 7 (**a7,b7**) days.

Vickers hardness using a HXD-1000TM/LCD Vickers microindenter (Shanghai Taiming Optical Instrument Co. Ltd., China) with a testing force of 2.94 N and loading time of 15 s.

Degradation behavior. The degradation behavior of the porous scaffolds was evaluated by measuring their weight loss in PBS according to the following procedure: The scaffolds (10 mm × 10 mm × 5 mm) were equally weighted placed in capped bottles containing 100 mL PBS, and then incubated in a rotary shaker (100 r/m) at 37 °C for different time intervals of 7, 14, 21 and 28 days. They were extracted at the end of each incubation period and washed three times with distilled water to remove ions absorbed on the surface, and then dried under electro-thermal blowing dry box to constant weight. The weight loss (WL) was denoted as $WL = (W_0 - W_t)/W_0 \times 100\%$, where W_0 was the dry weight before degradation, W_t was the dry weight after degradation. The surface morphologies of the dried scaffolds after soaking for different times were determined with SEM.

Filler and content	Processing method	Mechanical properties		
		Strength	Modulus	Hardness
1 wt% BNNSs + 7 wt% T-ZnO$_w$ Present study	Selective laser sintering	34.15 MPa	2.83 GPa	243.18 MPa
50 wt% nano- or micro-HAP rods [ref. 44]	Thermally induced phase separation method	14.9 or 13.7 MPa	8.67 or 4.61 MPa	—
20–50 wt% HAP particles [ref. 45]	Forging process	106.7 ± 3.7~115.3 ± 3.9 MPa	5.3 ± 0.09~6.5 ± 0.2 GPa	20.8 ± 1.1~26.3 ± 2.2 MPa
1–10 wt% nanodiamond [ref. 46]	Solution casting and compression molding	114 ± 23~118 ± 15 MPa	4.4 ± 0.4~5.4 ± 0.5 GPa	—
1–10 wt% nanodiamond (ND) [ref. 47]	—	—	2.6 ± 0.1~7.9 ± 0.1 GPa	0.05 ± 0.01~0.46 ± 0.05 GPa
1–10 wt% octadecylamine-functionalized ND [ref. 48]	—	—	4.2 ± 0.1~5.1 ± 0.1 GPa	0.21 ± 0.01~0.26 ± 0.01 GPa
30 wt% magnesium [ref. 49]	Solvent casting and molding by compression	101.3 ± 4.6 MPa	8.01 GPa	340 ± 20 MPa
10–50 wt% chitosan microspheres [ref. 50]	Thermally induced phase separation method	1.42–1.63 MPa	15.4–25.5 MPa	—
3 wt% multi-wall carbon nanotubes [ref. 51]	Solution casting	19 MPa	235 MPa	—
1 wt% single-walled carbon nanotubes [ref. 52]	Solvent casting method	28 MPa	820 MPa	—
30 wt% ZnO whiskers + 10% carbon fibers [ref. 53]	Melt-mixing and hot-pressing	80 MPa	8.9 GPa	—

Table 1. Comparison of mechanical properties achieved in scaffolds with literatures reported on PLLA composite with different fillers.

MG-63 cells adhesion and viability. MG-63 cells have similar characteristics of osteoblasts with the functions of synthesis, secretion and mineralization of bone matrix, making them attractive model for *in vitro* cell culture studies. The MG-63 cells were used to assay the cell adhesion and viability on the porous scaffolds of PLLA, PLLA/BN-0.75, PLLA/ZnO-5, PLLA/BN/ZnO-0.75-5 and PLLA/BN/ZnO-1-7 (10 mm × 10 mm × 5 mm). The cells were grown in DMEM supplemented with 10% FBS and 1% penicillin/streptomycin at 37 °C in a humidified 5% CO_2 atmosphere. Prior to cell seeding, the scaffolds were sterilized in 70% ethanol and transferred to 24-well plates. MG-63 cells were seeded onto each scaffold at a density of 4×10^5 cells. The culture medium was changed every other day.

The cell/scaffold constructs were taken out after 7 days of culturing and fixed in 2.5% glutaraldehyde for 20 min after incubation, and then washed with PBS three times and dehydrated in a series of graded ethanol for 10 min. They were gold-sputtered after drying in the dry box overnight and observed using SEM. The viability of MG-63 cells was studied using a live-dead fluorescence assay. The cell/scaffold constructs were rinsed with PBS three times after cell culture, and then exposed to 0.15 mm calcein-AM to target living cells and 2 mm ethidium homodimer-1 to target dead cells at 37 °C for 30 min followed by washing with PBS. Then they were analyzed using a fluorescence microscope (Olympus Co. Ltd., Tokyo, Japan) equipped with a digital camera (Olympus America Inc., Mel-ville, NY, USA).

HBMSCs proliferation and differentiation. HBMSCs are bone marrow-derived mesenchymal stem cells, and they may differentiate into osteoblasts only under induction conditions. They were used to evaluate the inductive osteogenic differentiation ability of the bone scaffolds with the addition of BN and ZnO, while MG-63 osteosarcoma cells did not have the ability to evaluate the inductive osteogenic differentiation ability. The hBMSCs were seeded into a 24-well plate preloaded with the scaffolds (10 mm × 10 mm × 5 mm) at the concentrations of 5×10^5 cells per scaffold and cultured at 37 °C in a humidified 5% CO_2 atmosphere for 1, 3, 5 and 7 days. The culture medium was changed every other day. After cell culture, the cell/scaffold constructs were fixed in 2.5% glutaraldehyde, washed with PBS and dehydrated through a graded ethanol series, coated with gold and observed with SEM.

The hBMSCs proliferation on the scaffolds was quantitatively evaluated by MTT assay. 100 μl of MTT solution was added into each well after cell culture for 1, 3, 5 and 7 days and incubated at 37 °C for 4 h. And then 600 μl of DMSO was added to dissolve the reaction product formazan after removal of supernatants. Meanwhile, the blank wells of cell culture plate were used as the positive control. 200 μl of solution was transferred into a new 96-well plate and the absorbance was assessed at a wavelength of 570 nm using an enzyme-labeled instrument (Amersham, UK).

The inductive ability of the scaffolds was determined by alkaline phosphatase (ALP) expression using a LabAssay™ ALP kit (Wako, Osaka, Japan) in accordance with the manufacturer's protocol. The cell/scaffold constructs were gently rinsed with PBS after cell culture and incubated in 0.1% Triton X-100 solution for 10 min. And then, 100 μl of lysate containing 100 μl of *p*-nitrophenyl phosphate (*p*NPP) was added to the solution and incubated for 60 min. The ALP activity was assayed by measuring the release of *p*-nitrophenol from *p*NPP.
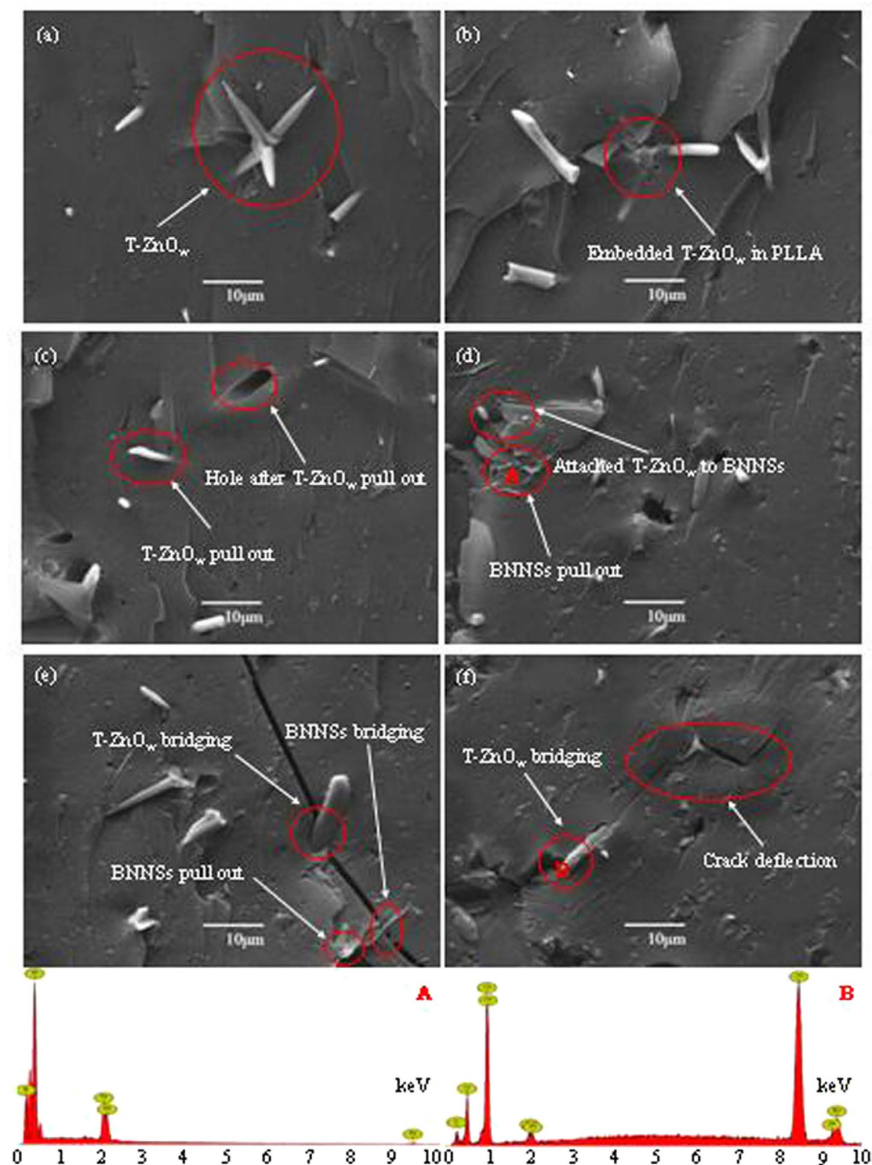
Figure 10. Fracture images and EDS spectra. Fracture images of the PLLA/BN/ZnO scaffolds (**a–f**), and EDS spectra of the element composite at the point A and B.

Statistical analysis. Data from all studies were analyzed using SPSS Statistics version 19 (IBM Co., USA). Results were expressed as mean ± standard deviation (SD). *Denotes a significant difference when $P < 0.05$, and **denotes a very significant difference when $P < 0.01$.

References

1. Hu, Y. *et al.* Facile fabrication of poly(ʟ-lactic acid)-grafted hydroxyapatite/poly(lactic-co-glycolic acid) scaffolds by pickering high internal phase emulsion templates. *ACS Appl. Mater. Inter.* **6,** 17166–17175 (2014).
2. Hu, Y., Zou, S., Chen, W., Tong, Z. & Wang, C. Mineralization and drug release of hydroxyapatite/poly(ʟ-lactic acid) nanocomposite scaffolds prepared by Pickering emulsion templating. *Colloid. Surface. B.* **122,** 559–565 (2014).
3. Yang, Y. *et al.* Research of osteoblastic induced rat bone marrow mesenchymal stem cells cultured on β-TCP/PLLA porous scaffold. *Int. J. Clin. Exp. Med.* **8,** 3202–3209 (2015).
4. Gui, H. *et al.* Effects of biodegradable imidazolium-based ionic liquid with ester group on the structure and properties of PLLA. *Macromol. Res.* **22,** 583–591 (2014).
5. Chen, P. *et al.* Greatly enhanced mechanical properties and heat distortion resistance of poly(ʟ-lactic acid) upon compositing with functionalized reduced graphene oxide. *J. Mater. Chem. A.* **1,** 9028–9032 (2013).
6. Jiang, T., Kuila, T., Kim, N. H., Ku, B. C. & Lee, J. H. Enhanced mechanical properties of silanized silica nanoparticle attached graphene oxide/epoxy composites. *Compos. Sci. Technol.* **79,** 115–125 (2013).
7. Lahiri, D. *et al.* Carbon nanotube reinforced polylactide-caprolactone copolymer: Mechanical strengthening and interaction with human osteoblasts *in vitro*. *ACS Appl. Mater. Inter.* **1,** 2470–2476 (2009).
8. El Achaby, M. & Qaiss, A. Processing and properties of polyethylene reinforced by graphene nanosheets and carbon nanotubes. *Mater. Design.* **44,** 81–89 (2013).

9. Dong, Y. *et al.* Polylactic acid (PLA) biocomposites reinforced with coir fibres: Evaluation of mechanical performance and multifunctional properties. *Compos. Part A-Appl. S.* **63,** 76–84 (2014).

10. Fang, Z. & Feng, Q. Improved mechanical properties of hydroxyapatite whisker-reinforced poly(L-lactic acid) scaffold by surface modification of hydroxyapatite. *Mater. Sci. Eng. C-Mater.* **35,** 190–194 (2014).

11. Shuai, C. *et al.* Graphene oxide reinforced poly (vinyl alcohol): nanocomposite scaffolds for tissue engineering applications. *RSC Adv.* **5,** 25416–25423 (2015).

12. Wang, X. *et al.* High-yield boron nitride nanosheets from 'chemical blowing': towards practical applications in polymer composites. *J. Phys-Condens. Mat.* **24,** 314205 (2012).

13. Ke, K., Pötschke, P., Jehnichen, D., Fischer, D. & Voit, B. Achieving β-phase poly (vinylidene fluoride) from melt cooling: Effect of surface functionalized carbon nanotubes. *Polymer.* **55,** 611–619 (2014).

14. Yang, X. *et al.* Synergetic effect of cyanogen functionalized carbon nanotube and graphene on the mechanical and thermal properties of poly (arylene ether nitrile). *J. Polym. Res.* **19,** 1–6 (2012).

15. Li, W., Dichiara, A. & Bai, J. Carbon nanotube-graphene nanoplatelet hybrids as high-performance multifunctional reinforcements in epoxy composites. *Compos. Sci. Technol.* **74,** 221–227 (2013).

16. Yang, S. Y. *et al.* Design and tailoring of a hierarchical graphene-carbon nanotube architecture for supercapacitors. *J. Mater. Chem.* **21,** 2374–2380 (2011).

17. Chatterjee, S. *et al.* Size and synergy effects of nanofiller hybrids including graphene nanoplatelets and carbon nanotubes in mechanical properties of epoxy composites. *Carbon.* **50,** 5380–5386 (2012).

18. Chatterjee, S., Nüesch, F. A. & Chu, B. T. T. Crystalline and tensile properties of carbon nanotube and graphene reinforced polyamide 12 fibers. *Chem. Phys. Lett.* **557,** 92–96 (2013).

19. Liu, F. *et al.* Cheap, gram-scale fabrication of BN nanosheets via substitution reaction of graphite powders and their use for mechanical reinforcement of polymers. *Sci. Rep-UK.* **4,** 4211 (2014).

20. Mortazavi, B. & Cuniberti, G. Mechanical properties of polycrystalline boron-nitride nanosheets. *RSC Adv.* **4,** 19137–19143 (2014).

21. Lahiri, D. *et al.* Boron nitride nanotube reinforced hydroxyapatite composite: mechanical and tribological performance and *in-vitro* biocompatibility to osteoblasts. *J. Mech, Behave. Biomed.* **4,** 44–56 (2011).

22. Lahiri, D. *et al.* Boron nitride nanotube reinforced polylactide–polycaprolactone copolymer composite: mechanical properties and cytocompatibility with osteoblasts and macrophages *in vitro. Acta Biomater.* **6,** 3524–3533 (2010).

23. Horvath, L. *et al. In vitro* investigation of the cellular toxicity of boron nitride nanotubes. *ACS Nano.* **5,** 3800–3810 (2011).

24. Ciofani, G., Raffa, V., Menciassi, A. & Cuschieri, A. Boron nitride nanotubes: an innovative tool for nanomedicine. *Nano Today.* **4,** 8–10 (2009).

25. Li, X. *et al.* Boron nitride nanotube-enhanced osteogenic differentiation of mesenchymal stem cells. *J. Biomed. Mater. Res. B* (2015).

26. Ni, H. Y., Wang, S. W., Zhou, Y. J. & Chen, J. The effect of fillers on the vulcanizing performances and mechanical properties of the fluoroelastomer. *Polym-Plast. Technol.* **49,** 1079–1086 (2010).

27. Yuan, J. *et al.* Effect of ZnO whisker content on sinterability and fracture behaviour of PZT peizoelectric composites. *J. Alloy. Compd.* **504,** 123–128 (2010).

28. Yuan, F. Y., Zhang, H. B., Li, X., Li, X. Z. & Yu, Z. Z. Synergistic effect of boron nitride flakes and tetrapod-shaped ZnO whiskers on the thermal conductivity of electrically insulating phenol formaldehyde composites. *Compos. Part A-Appl. S.* **53,** 137–144 (2013).

29. Niu, L. N. *et al.* Tetrapod-like zinc oxide whisker enhancement of resin composite. *J. Dent. Res.* **89,** 746–750 (2010).

30. Feng, P., Wei, P., Shuai, C. & Peng, S. Characterization of mechanical and biological properties of 3-D scaffolds reinforced with zinc oxide for bone tissue engineering. *Plos One.* **9,** e87755 (2014).

31. Augustine, R. *et al.* Electrospun polycaprolactone/ZnO nanocomposite membranes as biomaterials with antibacterial and cell adhesion properties. *J. Polym. Res.* **21,** 1–17 (2014).

32. Riaz, M. *et al. In vitro* evaluation of bioactivity of SiO$_2$-CaO-P$_2$O$_5$-Na$_2$O-CaF$_2$-ZnO glass-ceramics. *Mater. Sci-Poland.* **32,** 364–374 (2014).

33. Rabiee, S. M., Nazparvar, N. & Rajabi, M. Structural behavior and *in vitro* bioactivity evaluation of Sol-Gel derived glass-ceramics based on SiO$_2$-CaO-P$_2$O$_5$-ZnO system. *Silicon.* 1–9 (2015).

34. Feng, P., Niu, M., Gao, C., Peng, S. & Shuai, C. A novel two-step sintering for nano-hydroxyapatite scaffolds for bone tissue engineering. *Sci. Rep-UK.* **4,** 5599 (2014).

35. Tang, L. C. *et al.* The effect of graphene dispersion on the mechanical properties of graphene/epoxy composites. *Carbon.* **60,** 16–27 (2013).

36. Lee, A. S. Y., Chong, M. H., Park, M., Kim, H. Y. & Park, S. J. Effect of chemically reduced graphene oxide on epoxy nanocomposites for flexural behaviors. *Carbon Lett.* **15,** 67–70 (2014).

37. Yao, K. *et al.* Flammability properties and electromagnetic interference shielding of PVC/graphene composites containing Fe$_3$O$_4$ nanoparticles. *RSC Adv.* **5,** 31910–31919 (2015).

38. Şen, Ö. & Culha, M. Boron nitride nanotubes included thermally cross-linked gelatin-glucose scaffolds show improved properties. *Colloid. Surface. B.* **138,** 41–49 (2016).

39. Yakimova, R. *et al.* ZnO materials and surface tailoring for biosensing. *Front. Biosci.* **4,** 254–278 (2012).

40. Mallakpour, S. & Hatami, M. Optically active poly (amide-imide)/zinc oxide hybrid nanocomposites based on hydroxyphenyl benzamide segments: Compatibility by using 3-methacryloxypropyltrimethoxysilane coupling agent. *Polym. Sci. Ser. B.* **55,** 643–650 (2013).

41. Ikeda, T. *et al.* Fabrication and characteristics of chitosan sponge as a tissue engineering scaffold. *Biomed. Res. Int.* **2014,** 786892 (2014).

42. Wang, L., Ni, S. Q., Guo, C. & Qian, Y. One pot synthesis of ultrathin boron nitride nanosheet-supported nanoscale zerovalent iron for rapid debromination of polybrominated diphenyl ethers. *J. Mater. Chem. A.* **1,** 6379–6387 (2013).

43. Kim, D., Lee, Y., Seo, J., Han, H. & Khan, S. B. Preparation and properties of poly (urethane acrylate)(PUA) and tetrapod ZnO whisker (TZnO-W) composite films. *Polym. Int.* **62,** 257–265 (2013).

44. Nejati, E., Mirzadeh, H. & Zandi, M. Synthesis and characterization of nano-hydroxyapatite rods/poly(L-lactide acid) composite scaffolds for bone tissue engineering. *Compos. Part A-Appl. S.* **39,** 1589–1596 (2008).

45. Shikinami, Y. & Okuno, M. Bioresorbable devices made of forged composites of hydroxyapatite (HA) particles and poly-L-lactide (PLLA): Part I. Basic characteristics. *Biomaterials.* **20,** 859–877 (1999).

46. Zhang, Q. *et al.* Mechanical properties and biomineralization of multifunctional nanodiamond-PLLA composites for bone tissue engineering. *Biomaterials.* **33,** 5067–5075 (2012).

47. Zhang, Q. *et al.* Fluorescent PLLA-nanodiamond composites for bone tissue engineering. *Biomaterials.* **32,** 87–94 (2011)

48. Zhang, Q. *et al.* PLLA-Nanodiamond Composites and Their Application in Bone Tissue Engineering. *ASME.* 241–242 (2010).

49. Cifuentes, S. C. *et al.* Novel PLLA/magnesium composite for orthopedic applications: A proof of concept. *Mater. Lett.* **74,** 239–2420 (2012).

50. Niu, X., Feng, Q., Wang, M., Gou, X. & Zheng, Q. Porous nano-HA/collagen/PLLA scaffold containing chitosan microspheres for controlled delivery of synthetic peptide derived from BMP-2. *J. Control. Release.* **134,** 111–117 (2009).

51. Feng, J. *et al.* Preparation and characterization of magnetic multi-walled carbon nanotubes-poly(L-lactide) composite. *Mater. Sci. Eng. B-Solid.* **150,** 208–212 (2008).

52. Armentano, I. *et al.* Novel poly(L-lactide) PLLA/SWNTs nanocomposites for biomedical applications: material characterization and biocompatibility evaluation. *J. Biomat. Sci-Polym. E.* **22,** 541–556 (2011).
53. Nakamura, A. & Iji, M. How hybridization with zinc oxide whiskers and carbon fibers affects the thermal diffusivity and mechanical properties of poly(L-lactic acid) nanocomposites. *J. Mater. Sci.* **46,** 1439–1445 (2011).
54. Benhammou, A. *et al.* Mechanical behavior and ultrasonic non-destructive characterization of elastic properties of cordierite-based ceramics. *Ceram. Int.* **39,** 21–27 (2013).
55. He, G., Liu, P. & Tan, Q. Porous titanium materials with entangled wire structure for load-bearing biomedical applications. *J. Mech, Behave. Biomed.* **5,** 16–31 (2012).
56. Zhang, X. *et al.* Thermal, crystalline, and mechanical properties of octa (3-chloropropylsilsesquioxane)/poly(L-lactic acid) hybrid films. *J. App. Polym. Sci.* **122,** 296–303 (2011).
57. Han, H., Wang, X. & Wu, D. Mechanical properties, morphology and crystallization kinetic studies of bio-based thermoplastic composites of poly (butylene succinate) with recycled carbon fiber. *J. Chem. Technol. Biot.* **88,** 1200–1211 (2013).
58. Chand, N., Sharma, P. & Fahim, M. Tribology of maleic anhydride modified rice-husk filled polyvinylchloride. *Wear.* **269,** 847–853 (2010).
59. Canal, L. P., Pappas, G. & Botsis, J. Large scale fiber bridging in mode I intralaminar fracture. An embedded cell approach. *Compos. Sci. Technol.* **126,** 52–59 (2016).
60. Loos, M. R. *et al.* Enhancement of fatigue life of polyurethane composites containing carbon nanotubes. *Compos. Part B-Eng.* **44,** 740–744 (2013).
61. Davies, B. *et al.* Hypothesis: Bones toughness arises from the suppression of elastic waves. *Sci. Rep-UK.* **4,** 7538, (2014).
62. Wan, Y. *et al.* Adhesion and proliferation of OCT-1 osteoblast-like cells on micro-and nano-scale topography structured poly(L-lactide). *Biomaterials.* **26,** 4453–4459 (2005).
63. Wang, B., Cai, Q., Zhang, S., Yang, X. & Deng, X. The effect of poly(L-lactic acid) nanofiber orientation on osteogenic responses of human osteoblast-like MG63 cells. *J. Mech, Behave. Biomed.* **4,** 600–609 (2011).
64. Feng, P., Wei, P., Shuai, C. & Peng, S. Characterization of mechanical and biological properties of 3-D scaffolds reinforced with zinc oxide for bone tissue engineering. *Plos One.* **9,** e87755 (2014).
65. Fielding, G. & Bose, S. SiO₂ and ZnO dopants in three-dimensionally printed tricalcium phosphate bone tissue engineering scaffolds enhance osteogenesis and angiogenesis *in vivo*. *Acta Biomater.* **9,** 9137–9148 (2013).
66. Ciofani, G., Raffa, V., Menciassi, A. & Cuschieri, A. Cytocompatibility, interactions, and uptake of polyethyleneimine-coated boron nitride nanotubes by living cells: Confirmation of their potential for biomedical applications. *Biotechnol. Bioeng.* **101,** 850–858 (2008).
67. Lahiri, D. *et al.* Boron nitride nanotube reinforced polylactide-polycaprolactone copolymer composite: Mechanical properties and cytocompatibility with osteoblasts and macrophages *in vitro*. *Acta Biomater.* **6,** 3524–3533 (2010).
68. Ciofani, G., Raffa, V., Menciassi, A. & Dario, P. Preparation of boron nitride nanotubes aqueous dispersions for biological applications. *J. Nanosci. Nanotechno.* **8,** 6223–6231 (2008).
69. Lee, H. J., Kim, Y. B., Kim, S. H. & Kim, G. Mineralized biomimetic collagen/alginate/silica composite scaffolds fabricated by a low-temperature bio-plotting process for hard tissue regeneration: fabrication, characterisation and *in vitro* cellular activities. *J. Mater. Chem. B.* **2,** 5785–5798 (2014).
70. Farshid, B., Lalwani, G., Shir Mohammadi, M., Simonsen, J. & Sitharaman, B. Boron nitride nanotubes and nanoplatelets as reinforcing agents of polymeric matrices for bone tissue engineering. *J. Biomed. Mater. Res. B* (2015).
71. Jin, G. *et al.* Osteogenic activity and antibacterial effect of zinc ion implanted titanium. *Colloid. Surface. B.* **117,** 158–165 (2014).
72. Lu, H. *et al. In vitro* proliferation and osteogenic differentiation of human bone marrow-derived mesenchymal stem cells cultured with hardystonite (Ca₂ZnSi₂O₇) and β-TCP ceramics. *J. Biomater. Appl.* **25,** 39–56 (2010).

Acknowledgements

Author Contributions

P.F. and S.P. conceived and designed the research. P.F., C.G. and W.H. performed the microstructural and mechanical tests. S.P., P.W. and Y.D. performed the biological experiments. P.F., S.P. and C.S. analyzed the data and wrote the manuscript. All authors reviewed the manuscript.

Additional Information